Atmospheric phase screen estimation for land subsidence evaluation by InSAR time series analysis in Kurdistan, Iran

Haji-Aghajany, Saeid; Amerian, Yazdan

DOI
10.1016/j.jastp.2020.105314

Publication date
2020

Document Version
Accepted author manuscript

Published in
Journal of Atmospheric and Solar-Terrestrial Physics

Citation (APA)
Haji-Aghajany, S., & Amerian, Y. (2020). Atmospheric phase screen estimation for land subsidence evaluation by InSAR time series analysis in Kurdistan, Iran. *Journal of Atmospheric and Solar-Terrestrial Physics*, *205*, Article 105314. https://doi.org/10.1016/j.jastp.2020.105314

Atmospheric Phase Screen Estimation for Land Subsidence Evaluation by InSAR Time Series Analysis in Kurdistan, Iran

Saeid Haji-Aghajany[a,b], Yazdan Amerian[a]

[a]Faculty of Geodesy and Geomatics Engineering, K. N. Toosi University of Technology, Tehran, Iran

[b]Faculty of Civil Engineering and Geosciences, Delft University of Technology, Stevinweg 1, 2628 CN Delft, The Netherlands

s_h_aghajany@mail.kntu.ac.ir, s.hajiAghajany@tudelft.nl, amerian@kntu.ac.ir

Abstract

Atmospheric phase screen (APS) is one of the main error sources of interferometric synthetic aperture radar (InSAR) measurements. In order to accurately retrieve displacement fields, it is necessary to use advanced methods to eliminate the tropospheric effect of interferograms. In this paper, the land subsidence in Kurdistan province of Iran is investigated using Sentinel-1A acquisitions on a single track for the period 2014–2018. The accurate and applicable 3D ray tracing technique is used to accurately estimate the APS. The ERA-I reanalysis data generated by European Centre for Medium Range Weather Forecasts (ECMWF) are used to implement the 3D ray tracing technique. In order to determine the effect of using the 3D ray tracing technique, the APSs are also determined using a traditional approach called, spatiotemporal filters method. To evaluate the capability of the two methods, the results are compared with the weather research and forecasting model (WRF) model. Finally, the interferograms are corrected using APSs from 3D ray tracing technique and traditional method and the subsidence rate in the study area is computed. Comparing the subsidence rates obtained from two APS estimation methods with piezometric data, GPS and precise levelling observations shows that the 3D ray tracing technique is significantly more accurate than traditional method in computing InSAR displacement fields.

Keywords: InSAR, Atmospheric Phase Screen, 3D Ray Tracing, Spatiotemporal filters, Subsidence

1. Introduction

Aquifers are one of the most important and vital water resources for agriculture, drinking, industry. In recent decades, factors such as population growth, the development of industrial activities have led to the excessive extraction of groundwater. Therefore, aquifer depletion has caused land subsidence in different parts of the world (Gumilar, 2015). It can be said that subsidence is the sudden or gradual downward movement of the Earth surface due to human activities or natural causes. Land subsidence could cause serious damage to the stability of human made structures and aquifer and change in groundwater quality and generally vulnerability of plain against drought and ecosystem extinction. Therefore, land subsidence analysis is substantial point, especially in potential places.

Iran is a vast country that has been temporarily and spatially limited in water resources in recent decades due to excessive extraction of groundwater for urban development and industrial activities (Motagh et al., 2008). The study area of this paper is located in east of Sanandaj city in Kurdistan province in Iran. Land subsidence can be analyzed by hydrogeology techniques and also by geodetic methods like precise point positioning using global navigation satellite system (GNSS) and InSAR technique (Abidin, 2008). InSAR technique is a powerful and accurate method with high spatial resolution which is used to measure and analyze displacement or deformation on the Earth surface (Kumar, 2011).

Atmospheric phase delay is one of the main limitation of InSAR measurement (Zebker et al., 1997; Jolivet et al., 2014). This delay should be modeled and corrected. There are many instruments for estimating the tropospheric delay such as radiosonde, water vapor radiometer and meteorological satellites and sensors (Merrikhpour and Rahimzadegan, 2017; Merrikhpour and Rahimzadegan, 2019). Many previous studies have studied the mitigation of tropospheric effects using different methods. One approach is based on characterizing the statistical properties of phase delay patterns using or based on a connected stack of interferograms (Emardson et al., 2003; Foster et al., 2006; Li et al., 2006; Lauknes, 2011). Other approaches are based on the analysis of the relationship between delay and elevation (Remy et al., 2003; Cavalié et al., 2007; Elliott et al., 2008), based on external data (Wright et al., 2001; Fournier et al., 2011; Dee et al., 2011;

Catalao et al., 2011; Jolivet et al., 2014) and based on ray tracing technique (Hobiger et al., 2010; Haji-Aghajany et al., 2019).

Unlike most of the correction methods which are based on external data, there is a traditional approach called spatiotemporal filter method that uses interferometric combination of a series of SAR acquisitions to detect tropospheric effects. The main idea of these methods is based on the assumption that the atmospheric influence is randomly in time, whereas deformation signal correlates with time (Ferretti et al., 2001; Mora et al., 2003; Tang et al., 2016). Therefore, it is expected that the atmospheric effect can be eliminated by temporal filtering of large time series SAR acquisitions. Spectral diversity (SD) is another method that has recently been used to correct atmospheric effects (Jung and Lee, 2015; Gomba et al., 2016; Fattahi et al., 2017; Mastro et al., 2020).

In this paper, the quantitative and qualitative effect of the tropospheric delay in InSAR-derived subsidence is investigated. For this purpose, the powerful 3D ray tracing technique and spatiotemporal filter method are used to estimate APSs. To assess the obtained APSs from these two methods, they are compared with WRF model outputs. Then these estimations are applied to the obtained interferograms. Finally, the land subsidence rates which are computed using two APS estimation methods are compared with geodetic and piezometric data.

2. InSAR analysis

InSAR is one of the most powerful techniques to investigate the land displacement. This technique is based on the use of the phase of radar acquisitions (Hooper, 2008).

The differential SAR interferometry (DInSAR) method involves the processing of two radar acquisitions taken at two different times from a common area. The purpose of this process is to validate surface displacement occurred in time between two acquisitions. This method has two main disadvantages. First, atmospheric effect cannot be effectively eliminated. Second, temporal decorrelation between two acquisitions often decrease the quality of the results. This method is generally used to study the deformation caused by earthquake.

In the last two decades, Persistent scatterer interferometry (PSI) and small baseline subset (SBAS) have been developed to obtain deformation time series by using multi-temporal SAR acquisitions (Ferretti et al., 2001; Berardion, 2002). The PSI and SBAS methods are based on the use of the larger number of acquisitions and persist scatterer (PS) in the imaging area. By using the PSI method, it is possible to compute linear displacement velocity and to rebuild nonlinear time series of each PS. The SBAS approach works only on PSs that are coherent above a selected threshold on all interferograms (Samsonov, 2010). These techniques have a high accuracy in computing displacements such as subsidence over time in the form of time series (Ferretti et al., 2001; Berardion, 2002).

Recently developed InSAR processing approaches is related to combination of the PSI and SBAS methods and selecting PS (Hooper, 2008).

In all methods of InSAR, the basic observable is called an interferogram, which represents the per-pixel phase difference between two radar acquisitions. It should be noted that in InSAR the displacement of each PS is measured relative to a reference PS. The phase of the reference PS is set to zero. Therefore, the reference PS should be coherent and stable in all interferograms. After selecting PSs using amplitude dispersion index (ADI), for a given interferogram, considering the effects of the topography, atmospheric path delay, orbital error, and other thermal noise errors, the observed InSAR phase change can be expressed as (Zebker et al., 1997):

$$\Phi = \Phi_{def} + \Phi_{topo} + \Phi_{atm} + \Phi_{orbit} + \Phi_{noise} \quad (1)$$

Where Φ_{def} is the deformation phase along the LOS direction, Φ_{topo} is the phase resulted from the topography effect, Φ_{atm} is the phase resulted from the atmospheric delay, Φ_{orbit} is the phase due to orbital paths and Φ_{noise} is the phase related to other thermal noise errors. (Zebker et al., 1997). Because the purpose of the InSAR process is to extract the displacement, the other contributions in the InSAR phase should be modeled from auxiliary data and removed from Eq.1.

In this paper, the advanced spaceborne thermal emission and reflection radiometer (ASTER) digital elevation model (DEM) with resolution of 30 meter are used for the reduction of the topography effect and

orbital files are applied for orbital errors reduction. The important error in the InSAR observations which is difficult to model and may significantly affect the estimated displacement is due to the atmosphere. One of the purposes of this study is to review the methods for removing this error.

3. Tropospheric effect on a radar signal and its mitigation

Tropospheric effects on InSAR data are mainly due to variations in the refractive index. When a radar signal propagates through the inhomogeneous troposphere the velocity is lowered and the observations contaminated due to variable tropospheric effects (Jolivet et al., 2014). The variations of delays can cause a localized phase gradients in InSAR data. These variations are mainly due to the changes in tropospheric temperature, pressure and water vapor. Generally, temporal variations in pressure and temperature are not large enough to produce a localized phase gradients in InSAR data (Hanssen, 1998). The main reason for the effect of the troposphere on InSAR data is due to temporal variations in water vapor. Water vapor is usually observed in lower troposphere, where a strong turbulent mixing process occurs. Turbulent mixing can cause heterogeneity in the refractivity and can cause localized phase gradient in InSAR data (Hanssen, 1998; Hanssen, 2001). These phase gradient, which are caused by variations of tropospheric delay, called APS and must be estimated. In the following, the basics of the traditional method based on spatiotemporal filters and the 3D ray tracing technique based on eikonal equations will be introduced to compute the APSs.

3.1. APS estimation using spatiotemporal filters

The atmospheric conditions do not change in a very small area, so APS is low-pass in spatial domain. However, its temporal variations is like white noise. The non-linear displacement (NLD) is also low-pass in time (Fig.1). The extraction of APS requires low-pass filtering in the spatial domain.

Therefore, after applying a low-pass filter on interfrograms the APS (Ψ_{APS}) and the low frequency term of the NLD (Ψ_{NLD}) will be remained (Moyano Sanchez, 2009).

$$(\Psi)_{Low-Pass} = \Psi_{APS} + (\Psi_{NLD})_{Low-Pass} \quad (2)$$

Therefore, assuming APS is spatially correlated and temporally random unlike land displacement, it can be said that APS can be estimated using spatiotemporal filter. Finally, the temporally uncorrelated APS could be estimated using temporal filter. It should be noted that this assumption is not always correct because the

effects of seasonal variation of the atmospheric parameters, especially water vapor, could still remain (Hanssen, 1998; Ferretti et al. 2001; Moyano Sanchez, 2009).

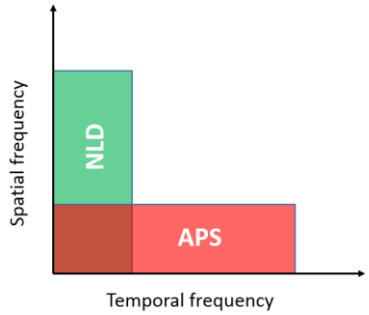

Figure 1. Spectral behavior of the APS and NLD (Moyano Sanchez, 2009).

In time domain, the NLD is low-pass whereas the APS is in the entire spectrum (Moyano Sanchez, 2009). To estimate the APS that is not overlapped with the NLD, it is necessary to use a temporal high-pass filter to the low-pass filter results. Finally, using both low-pass spatially and high-pass temporally filters the APS for each interferogram can be obtained. It should be noted that, the effect of APS estimation depends on the window size of the spatiotemporal filters. Smaller scale tropospheric effects may remain in the interferograms even after APS correction (Hanssen 2001). Therefore, the stratified APS will be corrected using ERA-Interim in the time series interferograms (Tang et al., 2016).

3.2. APS estimation using 3D ray tracing technique

Ray tracing is one of the most widely used and accurate techniques for determining tropospheric delay. this is the most precise technique to reconstruct the real path of signal propagation using atmospheric parameters which is widely used for determining tropospheric delay. Ray tracing technique is categorized in 2D and 3D methods. In 2D methods, ray tracing is performed in a fixed azimuth and in 3D method the path of a ray can be retrieved in 3D space (Hofmeister, 2016; Haji-Aghajany and Amerian, 2017; Haji-Aghajany and Amerian, 2018).

In this paper the new and powerful 3D ray tracing method is applied to compute the tropospheric delay for different radar acquisitions in different times. This method is based on the 3D reconstruction of the ray and the computation of the true distance traveled by it. The tropospheric delay can be measured by comparing the true distance traveled by the ray geometric distance. Finally, the tropospheric effects in each

interferogram can be obtained by comparing the delays obtained for the two master and slave acquisitions (Haji-Aghajany et al., 2019).

3D ray tracing method is based on the Eikonal equations. The Hamiltonian form of the Eikonal equations is as follows (Hofmeister, 2016; Haji-Aghajany and Amerian, 2017):

$$H(r,\nabla L) \equiv \frac{1}{a}\left\{(\nabla L.\nabla L)^{\frac{a}{2}} - n(r)^a\right\} = 0 \tag{3}$$

$$\frac{dr_i}{du} = \frac{\partial H}{\partial \nabla L_i} \quad , \quad \frac{d\nabla L_i}{du} = -\frac{\partial H}{\partial r_i} \quad , \quad \frac{dL_i}{du} = \nabla L_i . \frac{\partial H}{\partial \nabla L_i} \tag{4}$$

Where $H(r,\nabla L)$ is the Hamiltonian function, L is the length of the path travelled by the ray, ∇L is the components of signal directions, $\vec{r}$ is the position vector, $n(\vec{r})$ is the refractive index and a is an integer number. By setting this integer number, type of parameter of interest u is defined. By selecting a=1, Eq.3 can be rewritten as (Hofmeister, 2016; Haji-Aghajany and Amerian, 2017):

$$H(r,\theta,\lambda,L_r,L_\theta,L\lambda) \equiv (L_r^2 + \frac{1}{r^2}L_\theta^2 + \frac{L_\lambda^2}{r^2\sin^2\theta})^{\frac{1}{2}} - n(r,\theta,\lambda,t) \tag{5}$$

Where r is the radial distance, θ is co-latitude, λ is the longitude, L_r, L_θ and L_λ are the elements of the directions. Eq.5 is now substituted into Eq.4 to receive the six equations. To perform 3D ray tracing these equations must be solved using boundary conditions and initial values. In this paper the ERA-I data has been used to find initial value. More details about this method algorithm and its applications in tropospheric delay estimation and reconstruction of signal path in GNSS tropospheric sensing could be found in previous researches (Hobiger et al., 2008b; Hofmeister, 2016; Haji-Aghajany and Amerian, 2017; Haji-Aghajany and Amerian, 2018; Haji-Aghajany et al., 2020).

4. Study area and data set

The study area is located in the west of Iran, in Kurdistan province and in the east of Sanandaj city. This area is known as Dehgolan basin. Geologically, Dehgolan basin is part of Sanandaj-Sirjan zone and has the same geological history as Iran central zone. However, its structure is more similar to the Zagros (Alavi, 1994; Amini and Homayounfar, 2016). The maximum elevation of this area is about 2880 m from the sea level in the south of the basin. Based on De Martonne climate classification, this area has a dry and cool

climate. Due to the excessive extraction of groundwater, Dehgolan basin is on the list of forbidden plains in Iran and no more water extraction is allowed (Amini and Homayounfar, 2016). The location of the study area and its DEM are shown in Fig.2.

The launch of Sentinel-1 satellite was a new era for InSAR applications and time series analysis. The Sentinel missions are part of the European Union's earth observation programme which is named Copernicus and managed by the European Commission in partnership with the European Space Agency (ESA). The ESA is in charge of the technical development and maintenance of this satellite. The repeat interval of this satellite is 12 days. The data of an area are available in 6 days (ESA, 2017). To perform the InSAR analysis, the Sentinel-1A radar acquisitions from track 174 (ascending) between 2014 and 2018 are used.

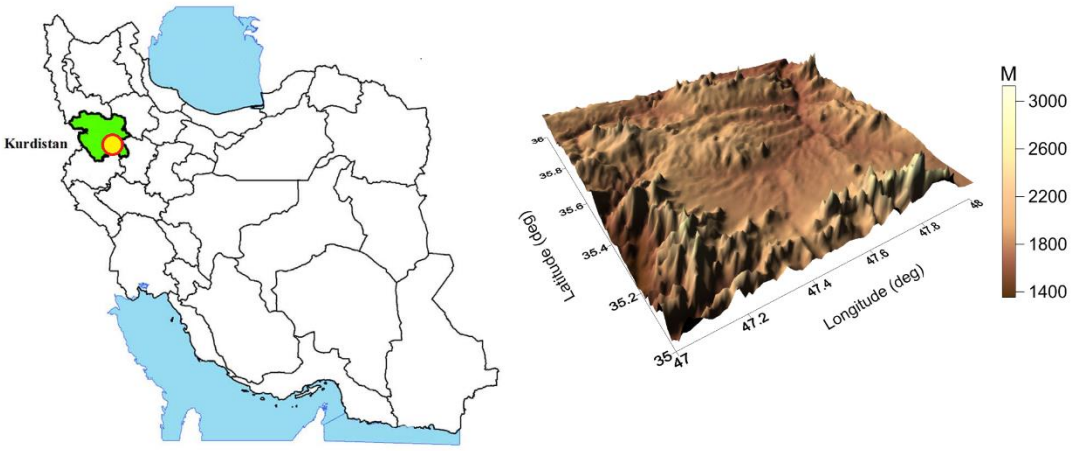

Figure 2. Location of the study area (yellow circle) and its DEM.

In this research, the ERA-I reanalysis model published by ECMWF has been used to perform 3D ray tracing technique. This model presented values of several meteorological data on 37 pressure levels. The spatial resolution of this data is about 75 km (Dee, 2011). Previous studies have shown that this data is very useful in a variety of fields, including geodynamics and geodesy (Haji-Aghajany et al., 2017: Haji-Aghajany et al., 2019). For each acquisition date, the ERA-I output which is the closest to the radar acquisition time is selected. The pressure, temperature and water vapor provided at each pressure level has been interpolated. Spline interpolation along altitude and kriging interpolation in the horizontal dimensions is applied.

The National Center for Environmental Prediction (NCEP) Climate Forecast System Reanalysis (CFSR) and NCEP's Global Forecast System analysis (GFS) data have been used to run the WRF model and validate the obtained APS (Rogers et al., 2001).

Piezometric data are one of the most useful tools to provide information about groundwater fluctuations, identifying groundwater recharge zones and interactions between groundwater and surface water. Piezometric data from groundwater wells are collected by the regional water organization. In this paper, these data are used to validate the InSAR displacement fields. In addition, precise levelling data and GPS observations are also used to evaluate the obtained displacement rate. The geographic location of the piezometric wells and GPS stations is visible in Fig.3.

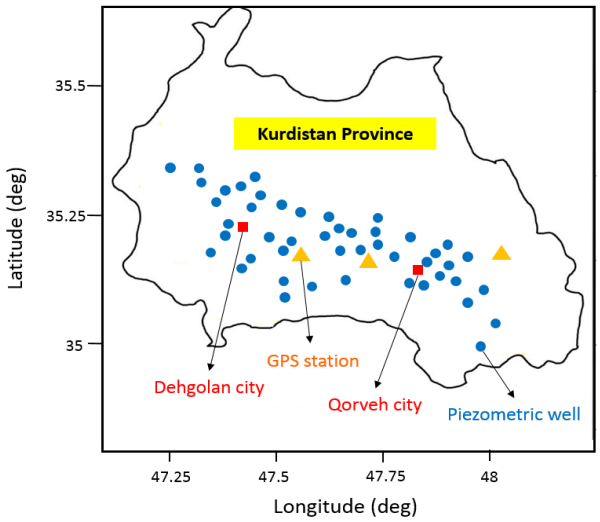

Figure 3. Spatial distribution of piezometric wells over the study area.

5. Analysis

A set of Sentinel-1A radar acquisitions have been used to InSAR analysis. In this processing, 0.42 have been selected for ADI and the scene has divided into 5×5 patches. Also, a reference PS has been selected with respect to the maximum of coherent pixels and smallest phase variance. For this selection, a group of PSs throughout the scenes have been tested. In order to obtain the displacement rate, additional effects must be removed from the interferograms. After eliminating the intrusive effects of topography and orbital error using the DEM and orbital data, the obtained interferograms only included atmospheric effects and

displacement phase. The atmospheric effect or APS on the obtained interferograms have been computed using two APS estimation methods. Samples of obtained APS are shown in Fig.4 and Fig.5.

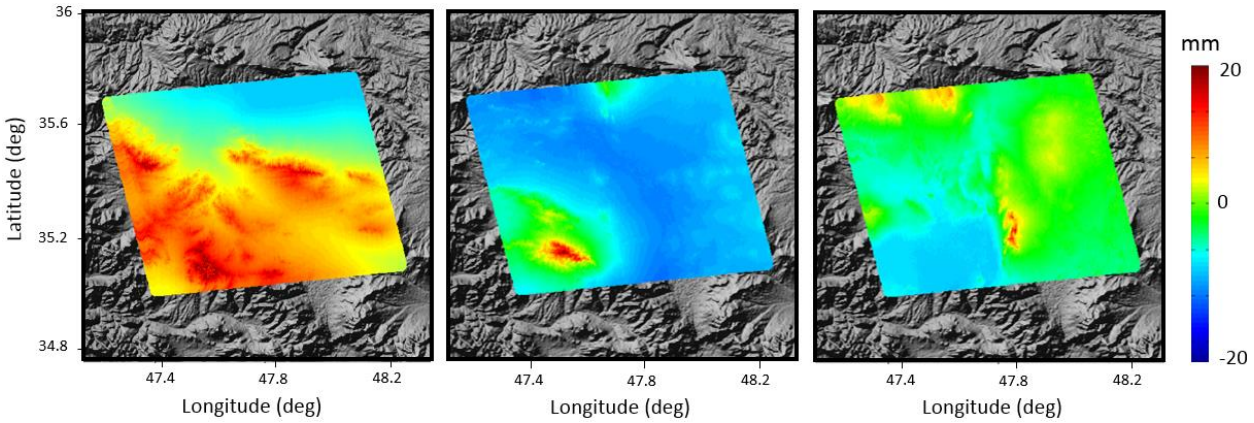

Figure 4. Samples of APS maps using spatiotemporal filters.

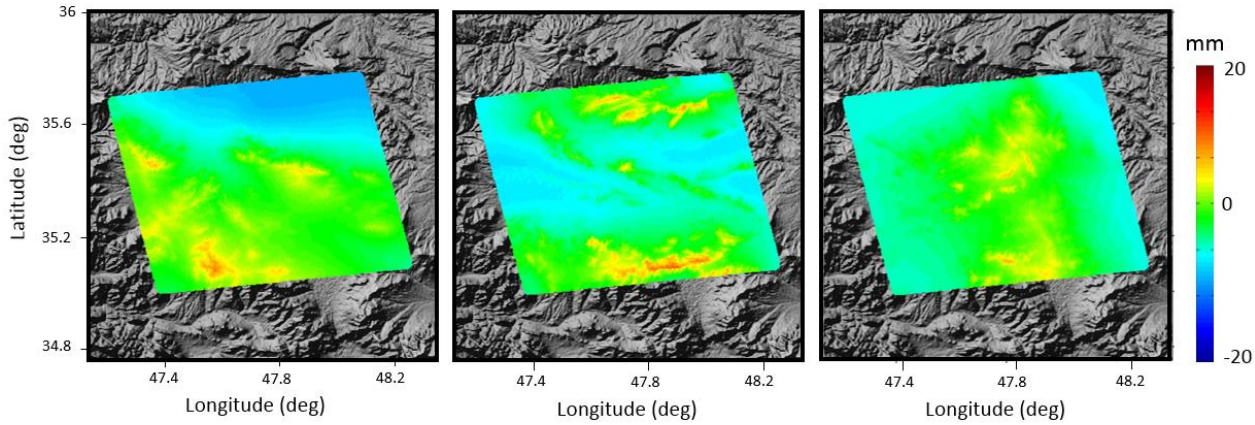

Figure 5. Samples of APS maps using 3D ray tracing technique.

In order to control and assess the results from two methods, they have been compared with WRF model outputs. To set the WRF model indicators in study area to obtain more accurate results, the library of Iran meteorological organization (IMO) for this indicators have been used. The statistical comparison of obtained APSs on 90480 PSs with WRF model outputs can be seen in Table.1.

Table 1. Statistical parameters and comparison of obtained APS maps

Method	Min (mm)	Max (mm)	Bias (mm)	Standard deviation (STD) (mm)	Correlation	Root mean square error (RMSE) (mm)
Spatiotemporal filter	-29.1	48.1	-4.7e-14	23.9	0.48	29.4
3D ray tracing	-32.1	39.4	3.7e-15	8.7	0.74	13.9

This comparison shows that the APSs obtained from the 3D ray tracing method are more consistent with the APSs obtained from the WRF model. After applying the estimated APSs by two mentioned methods on the obtained interferograms, the displacement rate of the area have been estimated (Fig.6). In order to better compare the results, two separate profiles have been considered on the obtained displacement fields. Fig.6 shows that in the case of using the spatiotemporal filter method corrections there are many subsidence and uplift signals in the area. The use of 3D ray tracing technique has reduced the number of these signals considerably. The high displacement rate and the high number of signals in the displacement rate map obtained by the spatiotemporal filter method could be related to the remaining atmospheric effects in the interferograms. Also, the use of 3D ray tracing technique may mask the subsidence and uplift signals and reduce their amount.

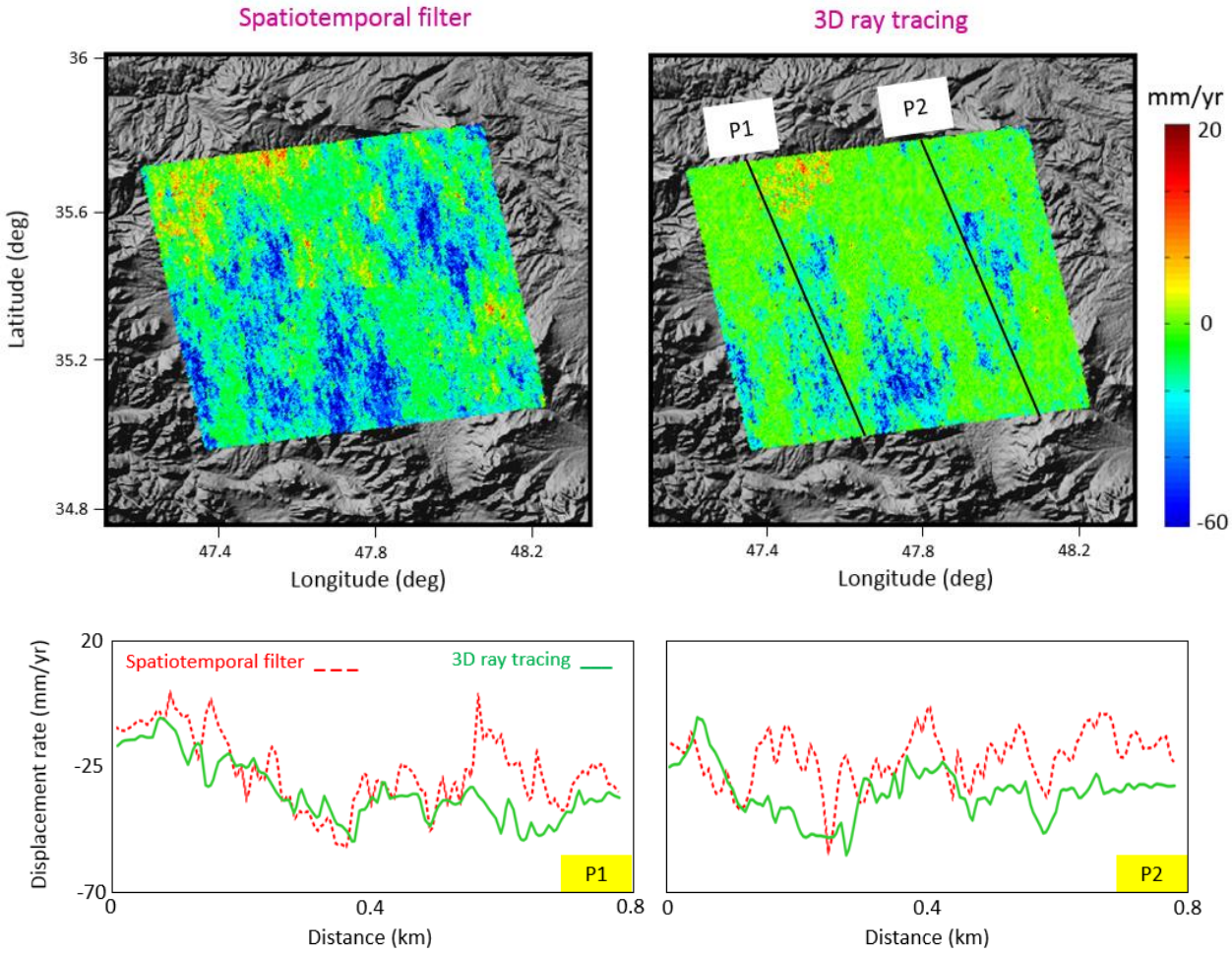

Figure 6. Obtained displacement rates and considered profiles.

In order to review the accuracy of the results, it is necessary to compare the obtained displacement rates with the displacement rates obtained from a series of accurate observations. The obtained displacement rate from two APS estimation methods, have been compared with precise levelling data (Fig.7). The RMSE of this comparison for 3D ray tracing is 9.47 mm/yr and for spatiotemporal filters is 19.51 mm/yr. Also, the displacement rate fluctuations obtained from the 3D ray tracing are more similar to the fluctuations of the precise levelling data. Generally, this comparison shows the efficiency of the 3D ray tracing technique in comparison with traditional method in InSAR APS estimation.

The time interval covered by precise levelling data and radar acquisitions is different and it may cause the different displacement rates from the two methods.

In addition, the displacement rates from two APS estimation methods have been compared with the displacement rates from GPS observations. Due to the time interval overlap of the GPS data and radar acquisitions, this comparison can provide more accurate and reliable results (Fig.7). The RMSE between GPS displacement rate and displacement rate from spatiotemporal filters is 12.09 mm/yr and the RMSE between GPS displacement rate and displacement rate from 3D ray tracing is 3.81 mm/yr. This comparison also shows the efficiency of the 3D ray tracing technique in comparison with traditional method in InSAR APS estimation.

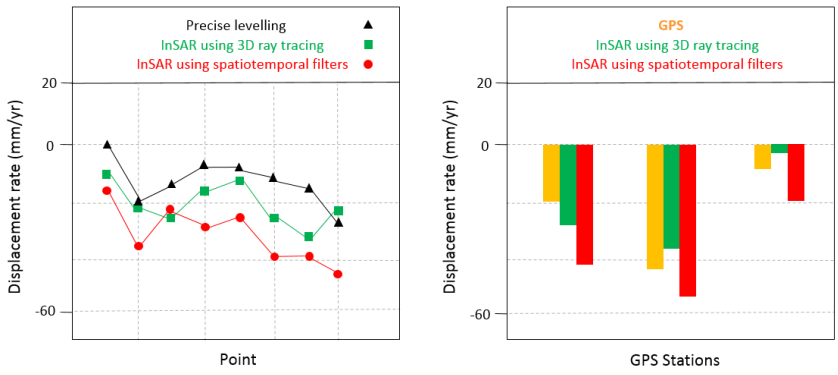

Figure 7. Comparison of obtained displacement rates with precise levelling and GPS data.

In order to better evaluate the obtained results, it is necessary to compare the InSAR time series with the piezometric data time series. Samples of this comparison at the position of 4 different piezometric wells can be seen in Fig.8.

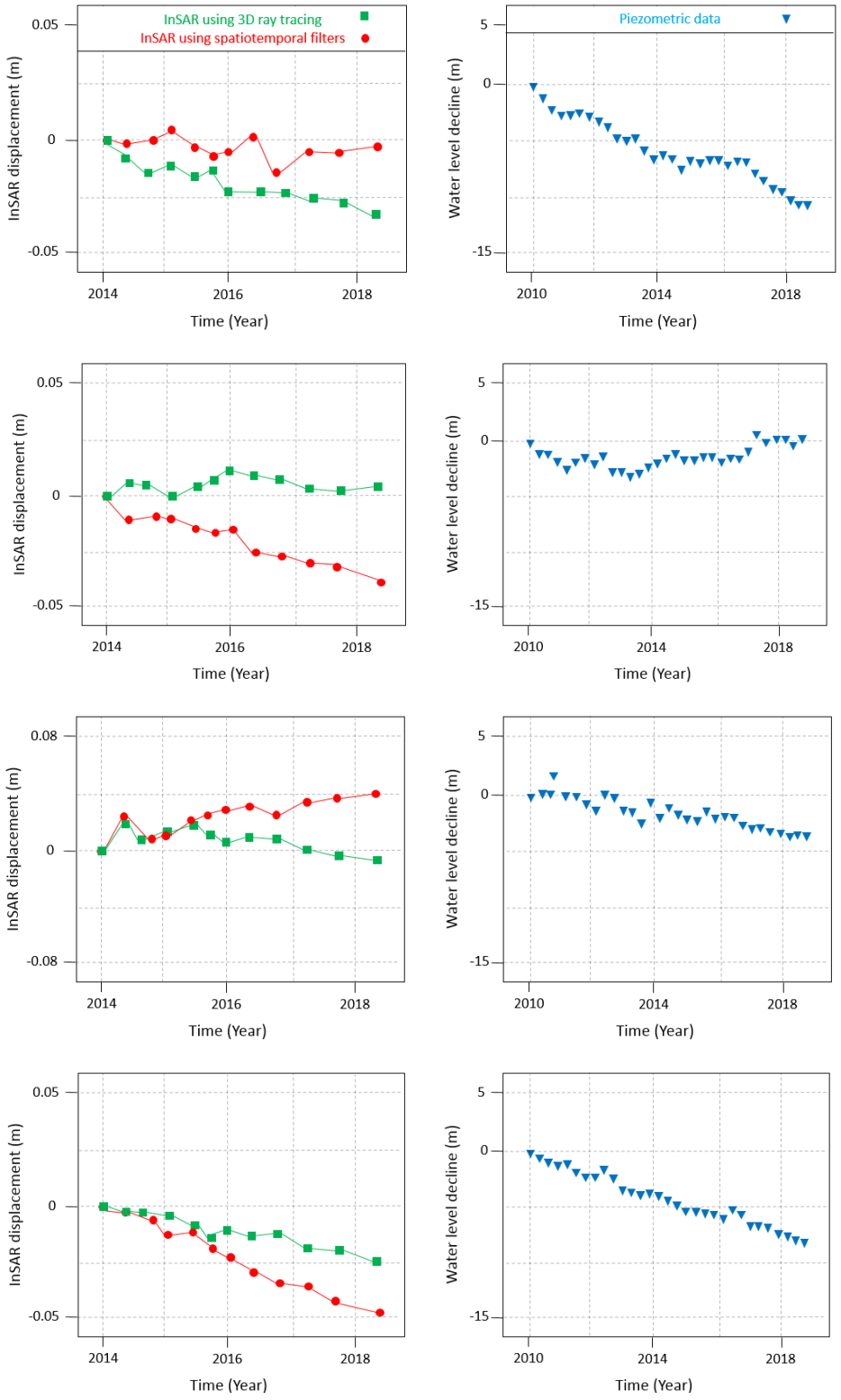

Figure 8. Samples of InSAR time-series and water level decline of four piezometric wells from up to down, respectively.

Fig.8 present groundwater level fluctuations of the piezometric wells and InSAR time series at location of these wells. For better presentation, the water level of piezometric wells has been set to zero. Therefore,

any negative value indicates the water level decline. The piezometric wells 1 and 4 shows the decline in water level caused by excessive water extraction. The well 3 also shows decline in water level, but less than the wells 1 and 4. The water level of well 2 does not demonstrates any decline. The existing fluctuation in this well is related to seasonal variations. The highest subsidence is observed at the location of wells 1 and 4, reflecting the maximum water level decline and aquifer depletion.

The obtained displacement from spatiotemporal filters at the location of well 1 does not show any subsidence, unlike displacement field from 3D ray tracing and water level. Piezometric data and displacement field from 3D ray tracing indicate that there is no subsidence at the location of well 2, but the displacement from spatiotemporal filters shows a clear subsidence. Also, at location of well 3, the results of spatiotemporal filters method do not fit well with other results and observations. Above mentioned results and comparisons indicate that the 3D ray tracing technique is more accurate and efficient than the spatiotemporal filters method in APS estimation. Because the 3D ray tracing technique reconstructs the exact path of the radar signal by considering all the conditions of the atmosphere and solving the Eikonal equations. In addition, this technique takes into account the lateral variations of the tropospheric parameters, which is neglected in other methods. It should be noted that the subsidence in this area due to the excessive water extraction is a great danger and should be considered.

6. Conclusions

Atmospheric effects are the main limiting factor in InSAR technique. These effects can cause errors of over one hundred millimeters to InSAR results. In this paper, the 3D ray tracing technique was used in order to estimate this effect and to achieve more accurate InSAR displacement fields. The results of the 3D ray tracing technique were compared with the results of the traditional spatiotemporal filters method. The estimated APS from the 3D ray tracing technique was much more consistent with the WRF model results. In order to investigate the effect of this method on displacement fields, an area was selected in the west of Iran, in Kurdistan province. After estimating the APS from two methods and correcting the interferograms, the time series and displacement rate were computed. Finally, comparison the results with piezometric data, GPS and precise levelling observations showed higher accuracy of the displacement filed obtained from

the 3D ray tracing technique compared to the traditional method. Despite the research done in this paper and previous studies, further investigations are still necessary to develop more effective methods for APS estimation to achieve more accurate InSAR displacement fields.

Acknowledgments

Authors would like to appreciate the ESA and ECMWF for providing the radar acquisitions and ERA-I data, respectively. Detailed and constructive reviews and editorial remarks are greatly appreciated.

References

Abidin, H. Z., Andreas, H., Gamal, M., Wirakusumah, A. D., Darmawan, D., Deguchi, T., & Maruyama, Y., 2008. Land subsidence characteristics of the Bandung Basin, Indonesia, as estimated from GPS and InSAR. Journal of Applied Geodesy, 2(3), 167-177.

Alavi M. 1994. Tectonics of the Zagros orogenic belt of Iran: New data and interpretations. Tectonophysics 229: 211–38.

Amini, A., Homayounfar, V., 2016. The groundwater balance in alluvial plain aquifer at Dehgolan, Kurdistan, Iran. Applied Water Science. doi:10.1007/s13201-016-0445-9.

Berardino, P.; Fornaro, G.; Lanari, R.; Sansosti, E. A new algorithm for surface deformation monitoring based on small baseline differential SAR interferograms. IEEE Trans. Geosci. Remote Sens. 2002, 40, 2375-2383.

Catalao, J.; Nico, G.; Hanssen, R.; Catita, C. Merging GPS and Atmospherically Corrected InSAR Data to Map 3-D Terrain Displacement Velocity. IEEE Trans. Geosci. Remote Sens. 2011, 49, 2354-2360.

Cavalié, O., Doin, M.P., Lasserre, C., Briole, P., 2007. Ground motion measurement in the Lake Mead area, Nevada, by differential synthetic aperture radar interferometry time series analysis: probing the lithosphere rheological structure. J. Geophys. Res. 112 (B3), B03403.doi:10.1029/2006JB004344.

Dee, D. P., and 35 co-authors. 2011). The ERA-Interim reanalysis: Configuration and performance of the data assimilation system, Q. J. R. Meteorol. Soc., 137(656), 553–597, doi:10.1002/qj.828.

Elliott, J,R. Biggs, J Parsons, B Wright, T J. 2008. InSAR slip rate determination on the AltynTagh Fault, northern Tibet, in the presence of topographically corre-lated atmospheric delays. Geophysical Research LETTERS ,35, L12309.

Emardson, T.R., Simons, M., Webb, F.H., 2003. Neutral atmospheric delay in interferometric synthetic aperture radar applications: statistical description and mitigation. J. Geophys. Res. 108 (B5), 2231.doi:10.1029/2002JB001781.

ESA, https://directory.eoportal.org/ (March 2017).

Fattahi, H.; Simons, M.; Agram, P. InSAR Time-Series Estimation of the Ionospheric Phase Delay: An Extension of the Split Range-Spectrum Technique. IEEE Trans. Geosci. Remote Sens. 2017, 55, 5984–5996. [CrossRef]

Ferretti, A., Prati, C., Rocca, F., 2001. Permanent scatters in SAR interferometry. IEEE Transactions on Geoscience and Remote Sensing 39 (1), 8–20.

Foster, J., B. Brooks, T. Cherubini, C. Shacat, S. Businger, and C. L. Werner., 2006. Mitigating atmospheric noise for InSAR using a high resolution weather model, Geophys. Res. Lett., 33, L16304, doi:10.1029/2006GL026781.

Fournier, T., M. E. Pritchard, and N. Finnegan (2011), Accounting for atmospheric delays in InSAR data in a search for long-wavelength deformation in South America, IEEE Trans. Geosci. Remote Sens., 49(10), 3856–3867, doi:10.1109/TGRS.2011.2139217.

Gomba, G.; Parizzi, A.; De Zan, F.; Eineder, M.; Bamler, R. Toward Operational Compensation of Ionospheric Effects in SAR Interferograms: The Split-Spectrum Method. IEEE Trans. Geosci. Remote Sens. 2016, 54, 1446–1461. [CrossRef]

Gumilar, I., Abidin, H. Z., Hutasoit, L. M., Hakim, D. M., Sidiq, T. P., & Andreas, H. (2015). Land subsidence in Bandung Basin and its possible caused factors. Procedia Earth and Planetary Science, 12, 47-62.

Haji-Aghajany, S.; Voosoghi, B.; Yazdian, A. Estimation of north Tabriz fault parameters using neural networks and 3D tropospherically corrected surface displacement field. Geomatics, Nat. Hazards Risk 2017, 8, 918–932, doi:10.1080/19475705.2017.1289248.

Haji-Aghajany, S.; Amerian, Y. Three dimensional ray tracing technique for tropospheric water vapor tomography using GPS measurements. J. Atmos. Solar Terr. Phys. 2017, 164, 81–88, doi:10.1016/j.jastp.2017.08.003.

Haji-Aghajany, S., Amerian, Y., 2018. Hybrid Regularized GPS Tropospheric Sensing Using 3-D Ray Tracing Technique. IEEE Geoscience and Remote Sensing Letters. 15(10):1475-1479. doi: 10.1109/LGRS.2018.2853183.

Haji-Aghajany, S., Voosoghi, B., Amerian, Y., 2019. Estimating the slip rate on the north Tabriz fault (Iran) from InSAR measurements with tropospheric correction using 3D ray tracing technique. Advances in Space Research. 64:11; 2199-2208; https://doi.org/10.1016/j.asr.2019.08.021.

Haji-Aghajany, S.; Amerian, Y.; Verhagen, S.; Rohm, W.; Ma, H. An Optimal Troposphere Tomography Technique Using the WRF Model Outputs and Topography of the Area. Remote Sens. 2020, 12, 1442. https://doi.org/10.3390/rs12091442.

Hanssen, R., 1998. Atmospheric heterogeneities in ERS tandem SAR interferometry. DEOS Report No.98.1, Delft University press: Delft, the Netherlands.

Hanssen, R. (Ed.), 2001. Radar Interferometry, Data Interpretation and Error Analysis. Kluwer Academic Publishers, p. 308.

Hobiger, T., Icikawa, R., Takasu, T., Koyama, Y., Kondo, T., 2008. Ray-traced troposphere slant delays for precise point positioning. Earth, planets and space 60 (5), e1–e4. issn: 1880-5981. doi: 10.1186/bf03352809.

Hobiger, T., Kinoshita, Y., Shimizu, S., Ichikawa, R., Furuya, M., Kondo, T and Koyama, Y., 2010. On the importance of accurately ray-traced troposphere corrections for interferometric SAR data. J. Geodesy, vol. 84, no. 9,pp. 537–546, DOI: 10.1007/s00190-010-0393-3.

Hofmeister, A., 2016. Determination of path delays in the atmsophere for geodetic VLBI bu means of ray tracing. Vienna university of technology. ISSN: 1811-8380.

Hooper, A., 2008. A multi-temporal InSAR method incorporating both persistent scatterer and small baseline approaches. Geophysical Research Letters 35, L16302.

Jolivet, R., P. S. Agram, N. Y. Lin, M. Simons, M. P. Doin, G. Peltzer, and Z. Li., 2014. Improving InSAR geodesy using global atmospheric models, J. Geophys. Res. Solid Earth, 119, 2324–2341, doi:10.1002/2013JB010588.

Jung, H.-S.; Lee, W.-J. An Improvement of Ionospheric Phase Correction by Multiple-Aperture Interferometry. IEEE Trans. Geosci. Remote Sens. 2015, 53, 4952–4960. [CrossRef]

Kumar, V., Venkataramana, G., & Høgda, K. A., 2011. Glacier surface velocity estimation using SAR interferometry technique applying ascending and descending passes in Himalayas. International Journal of Applied Earth Observation and Geoinformation, 13(4), 545-551.

Lauknes, T.R. InSAR Tropospheric Stratification Delays: Correction Using a Small Baseline Approach. IEEE Geosci. Remote Sens. Lett. 2011, 8, 1070-1074.

Li, Z., E. J. Fielding, P. Cross, and J.-P. Muller., 2006. Interferometric synthetic aperture radar atmospheric correction: GPS topography-dependent turbulence model, J. Geophys. Res., 111, B02404, doi:10.1029/2005JB003711.

Mastro P, Serio C, Masiello G, Pepe A. The Multiple Aperture SAR Interferometry (MAI) Technique for the Detection of Large Ground Displacement Dynamics: An Overview. Remote Sens. 2020, 12, 1189.

Merrikhpour, M., Rahimzadegan, M., 2017. Improving the Algorithm of Extracting Regional Total Precipitable Water Vapor Over Land From MODIS Images," in IEEE Transactions on Geoscience and Remote Sensing, vol. 55, no. 10, pp. 5889-5898, Oct. 2017. doi: 10.1109/TGR S.2017.2716414.

Merrikhpour, M., Rahimzadegan, M., 2019. Analysis of temporal and spatial variations of total precipitable water vapor in western Iran using radiosonde and MODIS measurements, Journal of Applied Remote Sensing 13(4), 044508. https://doi.org/10.1117/1.JRS.13.044508.

Motagh, M., Walter, T. R., Sharifi, M.A., Fielding, E., Schenk, A., Anderssohn, J., Zschau1, J., 2008. Land subsidence in Iran caused by widespread water reservoir overexploitation, Geophys. Res. Lett., VOL. 35, L16403.

Mora, O.; Mallorqui, J.J.; Broquetas, A. Linear and nonlinear terrain deformation maps from a reduced set of interferometric SAR images. IEEE Trans. Geosci. Remote Sens. 2003, 41, 2243-2253.

Moyano Sanchez, G., 2009. Atmosphere characterization with SAR interferometry, M.Sc. Dissertation, Universitat Politècnica de Catalunya.

Remy, D., Bonvalot, S., Briole, P., Murakami, M., 2003. Accurate measurement of tropospheric effects in volcanic areas from SAR interferometry data: application to Sakurajima volcano (Japan). Earth.Planet. Sci. Lett. 213, 299–310.

Rogers, E., et al., 2001. Changes to the NCEP Meso Eta Analysis and Forecast System: Increase in resolution , new cloud microphysics, modified precipitation assimilation, modified 3DVAR analysis. NWS Technical Procedures Bulletin. 488: p. 15.

Samsonov, S. Topographic Correction for ALOS PALSAR Interferometry. IEEE Trans. Geosci. Remote Sens. 2010, 48, 3020-3027.

Tang, W., Liao, M.S. & Yuan, P. 2016. Atmospheric correction in time -series SAR interferometry for land surface deformation mapping - A case study of Taiyuan, China. Advances in Space Research, 58, 310-325, doi: 10.1016/j.asr.2016.05.003.

Wright, T., Parsons, B., Fielding, E., 2001.Measurement of interseismic strain accu-mulation across the North Anatolian Fault by satellite radar interferometry.Geophysical Research Letters 28, 2117–2120.

Zebker, H.A., Rosen, P.A., Hensley, S., 1997. Atmospheric effects in interferometric synthetic aperture radar surface deformation and topographic maps. Journal of Geophysical Research 102 (2), 7547–7563.